Science of the Total Environment 694 (2019) 133564

Contents lists available at ScienceDirect

Science of the Total Environment

journal homepage: www.elsevier.com/locate/scitotenv

Nitrate effects on perchlorate reduction in a H_2/CO_2-based biofilm

Haixiang Li [a,1], Lijie Zhou [b,1], Hua Lin [a], Wenjie Zhang [a], Siqing Xia [c,*]

[a] Guangxi Collaborative Innovation Center for Water Pollution Control and Water Safety in Karst Area, Guilin University of Technology, Guilin 541004, PR China
[b] College of Chemistry and Environmental Engineering, Shenzhen University, Shenzhen 518060, PR China
[c] State Key Laboratory of Pollution Control and Resource Reuse, College of Environmental Science and Engineering, Tongji University, Shanghai 200092, PR China

HIGHLIGHTS

- Nitrate promotes perchlorate reduction at a NO_3^--N/ClO_4^- ratio lower than 5.
- Nitrate significantly inhibits perchlorate reduction at a NO_3^--N/ClO_4^- ratio higher than 10.
- Denitrification competes more strongly for H_2 than perchlorate.
- High nitrate loadings significantly shape the biofilm microbial community.
- Methyloversatilis and Zoogloea likely play important roles in perchlorate reduction.

GRAPHICAL ABSTRACT

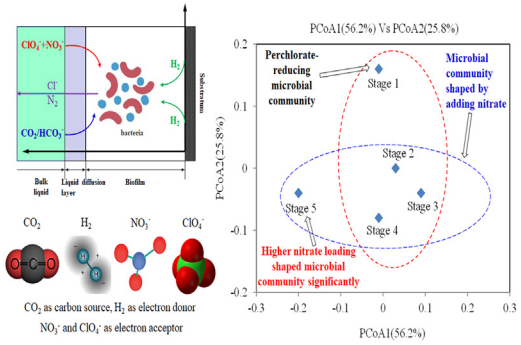

ARTICLE INFO

Article history:
Received 14 June 2019
Received in revised form 22 July 2019
Accepted 22 July 2019
Available online 23 July 2019

Editor: Huu Hao Ngo

Keywords:
Perchlorate reduction
Nitrate
Microorganism
H_2/CO_2-based membrane biofilm reactor

ABSTRACT

The H_2/CO_2-based membrane biofilm reactor (H_2/CO_2-MBfR) that effectively combines microporous diffusions of H_2 and CO_2 is efficient in removing perchlorate (ClO_4^-). Nitrate (NO_3^-) is a common oxidized contaminant frequently coexists with ClO_4^- in water, with the NO_3^- concentration in most ClO_4^--contaminated waters being several orders of magnitude higher than ClO_4^-. Determining the effect of NO_3^- on ClO_4^- reduction is a critical issue in practice. The ClO_4^- reduction performance, biofilm microbial community and influencing mechanism were investigated under a series of feed NO_3^- loadings in this work. ClO_4^- reduction was slightly promoted when NO_3^--N levels were <10 mg/L and inhibited at higher NO_3^--N levels. Denitrification competed more strongly for H_2 than ClO_4^- reduction, regardless of H_2 availability. A higher NO_3^--N loading was a strong driving force to change the biofilm microbial community. *Betaproteobacteria* were the dominant bacteria at all stages, and the biofilm reactor was enriched in *Methyloversatilis* and *Zoogloea* (31.9–56.5% and 10.6–25.8%, respectively). Changes in the relative amounts of *Methyloversatilis* and *Zoogloea* coincided with changes in the ClO_4^- fluxes and removal efficiencies and the relative abundances of nitrogen cycle functional genes. These results suggest that *Methyloversatilis* and *Zoogloea* likely follow independent reduction mechanisms for ClO_4^- removal.

1. Introduction

Perchlorate (ClO_4^-) is an emerging and persistent toxic contaminant that is widely used in the industrial production of leather, solid rocket fuel, fireworks, and electroplating (Cao et al., 2019). The extensive use and intrinsic properties (e.g., high solubility and non-reactivity) of

* Corresponding author.
E-mail address: siqingxia@gmail.com (S. Xia).
[1] Haixiang Li and Lijie Zhou contributed equally to this study.

https://doi.org/10.1016/j.scitotenv.2019.07.370
0048-9697/

ClO_4^- has resulted in its ubiquitous occurrence in receiving waters (Scheyett et al., 2011; Ye et al., 2012), leading to serious health issues such as abnormal metabolism, infant dysplasia, and thyroid cancer (Cartier et al., 2012). The US EPA has listed ClO_4^- as a priority pollutant and identified perchlorate as a drinking water contaminant (U.S. EPA, 2011). Therefore, robust approaches for the removal of ClO_4^- from water are urgently required to mitigate the environmental concerns associated with the utilization of this compound.

A considerable body of literature has extended our knowledge in terms of the microbiology, biochemistry, and genetics of microorganisms capable of reductively transforming ClO_4^- into chloride (Cl^-) (Ye et al., 2012; Zhao et al., 2013; Hutchison et al., 2017). It is well-known that ClO_4^- can be readily bioreduced to Cl^- under anaerobic conditions. The hydrogen-based membrane biofilm reactor (MBfR) is a novel water treatment technology to reduce oxidized pollutants, such as nitrate NO_3^-, ClO_4^-, selenite (SeO_4^{2-}), and Pd (II)) in water (Nerenberg and Martin, 2012; Zhao et al., 2013; Lai et al., 2014; Zhou et al., 2016; Li et al., 2018). It has major advantages of no secondary pollution, low biological yield, cost-effectiveness, high gas diffusion efficiency, and a small footprint (Nerenberg and Martin, 2012). In recent years, a simultaneous hydrogen and carbon dioxide diffusion membrane biofilm reactor (H_2/CO_2-MBfR) has been developed, which effectively integrates a microporous diffusion process for H_2/CO_2 (Xia et al., 2015, 2016). In the system, the diffusion of CO_2 through micropores maximizes the utilization efficiency of CO_2 in the reactor, thereby effectively overcoming issues such as inorganic carbon source supply, sharp increases in pH, and mineral precipitation on the membrane surface (Xia et al., 2016).

NO_3^- is a common oxidizing contaminant that frequently coexists with ClO_4^- in water because of the utilization of agricultural fertilizers (Wan et al., 2017; Sevdaa et al., 2018). The concentration of NO_3^- in most ClO_4^--contaminated waters is often several orders of magnitude higher than that of ClO_4^- (Kimbrough and Parekh, 2007; Fabro et al., 2015). NO_3^- and ClO_4^- possess similar chemical properties and reduction potentials (ClO_4^-/Cl^- pair: 1.28 V and NO_3^-/N_2 pair: 1.25 V) (Cecconet et al., 2018). As revealed in the literature, many isolated ClO_4^- reducing bacteria play a role in denitrification, and some bacteria that are mostly involved in denitrification can also participate in the reduction of ClO_4^- (Choi and Silverstein, 2008). Previous studies have shown that ClO_4^- and NO_3^- can be simultaneously removed by ClO_4^--degrading bacteria by the same NO_3^- reductase enzyme (Herman and Frankenberger, 1999; Logan and Lapoint, 2002). Moreover, bacteria involved in ClO_4^- reduction and denitrifying bacteria have similar energy metabolisms. While NO_3^- influences ClO_4^- reduction, ClO_4^- also impacts denitrification (Herman and Frankenberger, 1999). In the studies about NO_3^- and ClO_4^- reduction system, it was also found that pH change might induce biofilm to shit from nitrate to perchlorate reduction (Shea et al., 2008; Butler et al., 2010). Thus, these findings suggest that when ClO_4^- and NO_3^- coexist, a significant interaction between denitrification and ClO_4^- reduction occurs in the biofilm. Moreover, nitrite and nitrous oxide are the intermediate nitrogen forms of denitrification in MBfR, while nitrite has been related to carcinogenicity and nitrous oxide is a known greenhouse gas (Fan and Steinberg, 1996; Sabba et al., 2015). Consequently, the interaction between denitrification and ClO_4^- reduction need to be considered in MBfR when ClO_4^- and NO_3^- coexist, in case the production of nitrite and nitrous oxide.

When bioreactor systems are used to remove ClO_4^-, it is important to avoid inhibition of ClO_4^- reduction by NO_3^-. However, no systematic and quantitative analyses have been conducted on the effect of NO_3^- on the reduction of ClO_4^-, and no consistent conclusions on the mechanisms responsible for the inhibitory or promoting effects of NO_3^- on ClO_4^- reduction have been obtained. For example, some studies suggest that high concentrations of NO_3^--N (>10 mg/L) can inhibit the degradation of ClO_4^- (Herman and Frankenberger, 1999; Choi and Silverstein, 2008; London et al., 2011), while other studies report that low concentrations of NO_3^--N (<5 mg/L) can promote the degradation of ClO_4^- (Xu et al., 2004; Tang et al., 2012a, 2012b; Zhu et al., 2016).

While the effect of NO_3^- on ClO_4^- reduction in H_2 (Zhao et al., 2011; Tang et al., 2012a, 2012b) and organic electron donor (Zhu et al., 2016) bioreactors has been widely studied, the sharp increases in pH in the biofilm, which occur as a result of the reduction processes, remain unresolved, and have a negative impact on the assessment of ClO_4^- reduction. The weak acidity of CO_2 can be used to control the pH in the biofilm while simultaneously serving as a carbon source for microbial growth. Additionally, few investigations have focused on the effect of NO_3^- on ClO_4^- reduction and the biofilm microbial community in H_2/CO_2-MBfR systems. Thus, the first objective was to develop a bench-scale H_2/CO_2-MBfR to investigate the effect of NO_3^- concentration on the ClO_4^- reduction performance. The second objective was to identify changes in the biofilm microbial community structure with NO_3^- loading changes. Finally, the mechanisms responsible for the effect of NO_3^- on ClO_4^- reduction were analyzed.

2. Materials and methods

2.1. H_2/CO_2-MBfR setup

The H_2/CO_2-MBfR setup is shown in Fig. 1. A hollow fiber membrane module was fixed at both ends of the cylinder as a carrier for microbial growth. The hydrophobic hollow fibers were novel materials composed of polyvinyl chloride (PVC) manufactured by Litree Company (Suzhou, China), and the CO_2 microporous diffusion tube was also made of PVC. Pure H_2 diffuses from the membrane pore to the outside of the membrane without forming bubbles and is subsequently consumed by the microorganisms (biofilm) attached to the outer surface of the membranes as an electron donor. Pure CO_2 was delivered by the diffusion tube to the liquid and the biofilm attached to the hollow fibers. The physical characteristics of the H_2/CO_2-MBfR are listed in Table 1.

2.2. Feed medium, H_2/CO_2-MBfR startup and continuous operation

The synthetic feed medium was prepared with different ClO_4^- and NO_3^--N concentrations as previously described (Li et al., 2018). Detailed information is provided in Supplementary data. The H_2/CO_2-MBfR was inoculated with anaerobic activated sludge from a domestic sewage treatment plant (Guilin, Guangxi, China). The activated sludge was allowed to settle for 30 min, after which a 30 mL mixture at the solid–liquid interface was inoculated into the reactor to culture the biofilm. After inoculation, the H_2/CO_2-MBfR was started when H_2 and CO_2 were added to the fibers at 0.01 MPa with an inflow rate of 0.5 mL/min. The pH of the medium was adjusted to ca. 7.2 by a PHS-3C type pH meter, while KH_2PO_4 and Na_2HPO_4 acted as a buffer media to maintain a nearly neutral pH of the liquid. During this period, no ClO_4^- was added to the influent, but 1 mg/L of NO_3^--N was already present in the influent as a nitrogen source. Once the effluent NO_3^--N concentrations were stabilized, the influent flow rate was increased to 2.0 mL/min. Once NO_3^--N was completely removed from the effluent, the outer surfaces of the membranes showed a layer of yellow-brown biomass. Once the biofilm was formed, H_2 and CO_2 were supplied to the fibers at 0.04 and 0.01 MPa, respectively. The influent contained varied amounts of ClO_4^- (150 and 200 μg/L), which were supplied continuously at 2.0 mL/min to enhance the biofilm enrichment. The effluent ClO_4^- concentration reached a steady-state after about 80 days.

A series of long-term tests were conducted to evaluate the effects of NO_3^- on ClO_4^- degradation for 200 days (Table 2). In these experiments, the influent NO_3^--N concentrations were set to 1, 5, 10, 20, and 50 mg/L in stages 1, 2, 3, 4, and 5, respectively. In addition, the H_2 pressure was fixed to 0.04 MPa, the CO_2 pressure was set to 0.01 MPa, pH was 7.2, the inflow velocity was 2.0 mL/min, and the influent ClO_4^- concentration was 2000 μg/L. On average, 40 days for each test condition was found to be sufficient for the system to reach a pseudo steady-state, and for the liquid concentration to achieve a stable state. During this 40-day period, the biomass did not change significantly (Xia et al.,

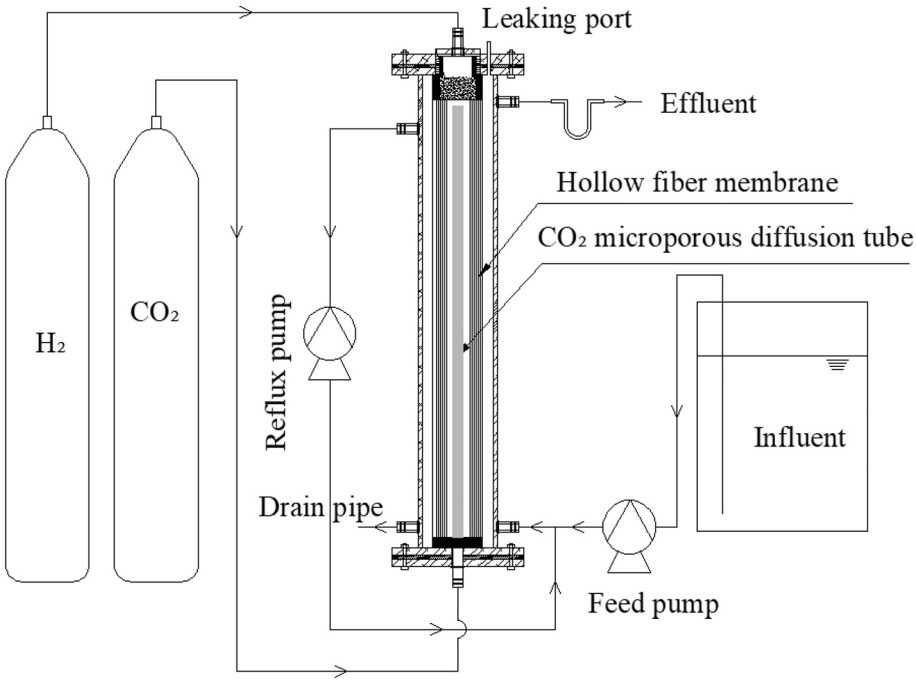

Fig. 1. Scheme of the bench-scale H_2/CO_2-MBfR used to investigate perchlorate reduction.

2011). During the last week of each stage, the concentrations of NO_3^--N, ClO_4^-, and Cl^- in the effluent reached steady-state values. The effluent concentrations in the last week of each stage were calculated to evaluate changes in the flux as described in Section 2.5.

2.3. Routine analysis and flux calculations

All liquid samples were collected and analyzed by the methods described in the Supplementary data. The fluxes of NO_3^--N and ClO_4^- in different steady stages were calculated using Eq. (1) to examine the effects of NO_3^- on ClO_4^- bioreduction. The normalization of the flux provided a simple measure of the intrinsic kinetics for given experimental conditions. This process was based on a pseudo first-order representation of the acceptor flux (J) in terms of the effluent acceptor concentration (S_e), as depicted in Eq. (2) (Chung and Rittmann, 2007). To investigate the competitive capacities for H_2 of these electron acceptors, the electron-equivalent flux (Eeq) and the reaction order of the electron acceptor (k') were calculated according to Eqs. (3) and (4), respectively (Rittmann and McCarty, 2001).

$$J = \frac{Q \times (S_i - S_e)}{A} \quad (1)$$

$$k = \frac{J}{S_e} \quad (2)$$

$$Eeq = \frac{J}{EW_s} = \frac{Q \times (S_i - S_e)}{A \times EW_s} \quad (3)$$

$$k' = \frac{d(\lg J)}{d(\lg S_e)} \quad (4)$$

where S_i and S_e are the influent and effluent NO_3^--N or ClO_4^- concentrations (g/m^3), respectively; J is the acceptor removal flux in the biofilm ($g/m^2 \cdot d$); Q is the flow rate of the influent (m^3/d); A is the biofilm surface area (m^2); k is the intrinsic lumped rate coefficient indicating the normalized flux (m/d); Eeq is electron-equivalent flux ($eq/m^2 \cdot d$); and EW_s is the g/e^- equivalent required for the complete reduction of the electron acceptor (2.8 g/e^- for NO_3^--N to be reduced to N_2, and 12.4 g/e^- for ClO_4^- to be reduced to Cl^-).

The actual H_2 consumption fluxes were calculated ($J_{H_2} = J_{NO_3} \times 3.03 \times 2/14 + J_{ClO_4} \times 5.48 \times 2/99.5$) from the removal fluxes of the oxidized compounds and the reaction stoichiometry shown in Eqs. (5) and (6). The delivery capacity of the PVC hollow fibers (maximum H_2 diffusion flux) was assessed as previously reported (Tang et al., 2012a, 2012b; Xia et al., 2015). A maximum H_2 diffusion flux of 0.246 g $H_2/m^2 \cdot d$ was obtained for the applied H_2 pressure of 0.04 MPa (Table 3). To determine whether the H_2 delivery was limiting, the actual H_2 flux was

Table 1
Physical characteristics of the H_2/CO_2-MBfR system.

Physical characteristics	Units	Value
Reactor height	cm	64
Reactor inner diameter	mm	6
Reactor available volume	L	1.8
Inflow velocity	mL/min	2
Reflux velocity	mL/min	20
Hydraulic residence time (HRT)	h	15
Number of hollow fibers	bunch	120
Membrane active length	cm	50
Membrane inner diameter	mm	1
Membrane outer diameter	mm	1.5
Membrane pore size	μm	0.02
Membrane active surface area	m^2	0.28
CO_2 microporous diffusion tube pore size	μm	10

Table 2
Series of long-term test conditions investigating nitrate effects on perchlorate degradation.

Stages	Periods (days)	Influent NO_3^--N (mg/L)	H_2 pressure (MPa)	CO_2 pressure (MPa)	Inflow velocity (mL/min)	pH	Influent ClO_4^- (μg/L)
1	1–40	1					
2	41–80	5					
3	81–120	10	0.04	0.01	2.0	7.2	2000
4	121–160	20					
5	161–200	50					

Table 3
Summary of the electron-equivalent fluxes and H_2 fluxes at steady states in long-term experiments.

Stages	Electron-equivalent fluxes ($eq/m^2 \cdot d$)			Distribution of electron-equivalent fluxes		Actual H_2 consumption fluxes (g $H_2/m^2 \cdot d$)			Maximum H_2 diffusion flux (g $H_2/m^2 \cdot d$)
	ClO_4^-	NO_3^--N	total	ClO_4^-	NO_3^--N	ClO_4^-	NO_3^--N	total	
1	0.0017	0.0038	0.0055	30.3%	69.7%	0.0145	0.0046	0.0191	0.246
2	0.0017	0.0191	0.0208	8.0%	92.0%	0.0147	0.0231	0.0378	0.246
3	0.0017	0.0381	0.0398	4.2%	95.8%	0.0146	0.0461	0.0607	0.246
4	0.0015	0.0748	0.0763	2.0%	98.0%	0.0121	0.0907	0.1028	0.246
5	0.0011	0.1820	0.1831	0.6%	99.4%	0.0094	0.2117	0.2211	0.246

compared to the maximum H_2 diffusion flux at the applied H_2 pressure.

$$NO_3^- + 3.03H_2 + 0.23CO_2 + H^+ = 0.48N_2 + 0.046C_5H_7O_2N + 3.37H_2O \quad (5)$$

$$ClO_4^- + 5.48H_2 + 0.11H^+ + 0.11NO_3^- + 0.53CO_2 = Cl^- + 5.15H_2O + 0.11C_5H_7O_2N \quad (6)$$

2.4. Biofilm sampling, high-throughput sequencing and analysis

Biofilm samples were collected for all stages when the performance of the reactors was at a steady state as revealed by stable concentrations of NO_3^--N, ClO_4^-, and Cl^- in the effluent. For each collection, three hollow fibers (10 cm in length) were cut into short pieces (ca. 1 cm) from different locations on the membrane module, and separated by ultrasonic treatment (SK3300-35 KHz, China). The biofilm samples were washed with TENP buffer and re-suspended with sodium phosphate buffer before DNA extraction.

The microbial community was analyzed by 16S rRNA gene cloning and amplicon pyrosequencing. Bacterial 16S rRNA gene fragments were PCR amplified using primers 341F and 805R. The PCR reaction system contained 15 μL 2 × Taq master Mix, 1 μL Primer F (10 μM), 1 μL Primer R (10 μM), 20 ng Genomic DNA, and 30 μL of ddH_2O. The PCR reaction conditions were as follows: 94 °C for 3 min; five cycles at 94 °C for 30 s, 45 °C for 20 s, and at 65 °C for 30 s; 20 cycles at 94 °C for 20 s, 55 °C for 20 s, and at 72 °C for 30 s; and then a final extension at 72 °C for 5 min. Amplicon pyrosequencing was conducted by Sangon Biotech (Shanghai) Co., Ltd. (Shanghai, China), using an Illumina Miseq™ sequencing system (Illumina, USA). Detailed information on sequencing analysis is provided in Supplementary data.

3. Results and discussion

3.1. Biofilm performance for NO_3^- and ClO_4^- reductions

The operation of the H_2/CO_2-MBfR started to grow the biofilm and reduce ClO_4^- (Fig. S1). After 80 days of biofilm enrichment, the influent NO_3^--N concentrations were set to 1, 5, 10, 20, and 50 mg/L, with a H_2/CO_2 pressure of 0.04/0.01 MPa and an influent ClO_4^- concentration of 2000 μg/L. Fig. 2(a) shows concentrations of ClO_4^-, NO_3^--N, and transformed Cl^- in the effluent along with concentrations of ClO_4^- and NO_3^--N in the influent. Fig. 2(b) shows the ClO_4^- and NO_3^--N removal percentages and Cl^- transformation percentages during the five stages.

In stage 1, strong ClO_4^- reduction started 3 days after adding ClO_4^- to the influent. The effluent ClO_4^- concentration reached 931 μg/L (55.4% removal of ClO_4^-) accompanying by an increase in the effluent Cl^- concentration. At the last five days of stage 1, 97% of the ClO_4^- and nearly 100% of the NO_3^--N were reduced. In stage 2, ClO_4^- reduction was slightly enhanced from day 55 (the ClO_4^- removal approached 99%, as did the NO_3^--N removal). In stage 3 (days 113–120), 98% of the ClO_4^- was removed with 30% Cl^- conversion. In stage 4, the influent NO_3^--N concentration increased to 20 mg/L and the extent of the ClO_4^- reduction declined dramatically within 3 days (68% removal of ClO_4^- and the Cl^- conversion reached 12%). After approximately 36 days of operation in stage 4, ClO_4^- reduction increased again to ca. 81% (days 156–160). In stage 5, 50 mg/L of NO_3^--N significantly inhibited ClO_4^- reduction, and the effluent ClO_4^- concentration increased to 736 μg/L (63% removal of ClO_4^-), corresponding to a 19.6% Cl^- conversion. NO_3^--N was simultaneously reduced at 90% to concentrations lower than 5 mg/L. In addition, nitrite, nitric oxide, nitrous oxide are the known intermediate nitrogen forms in the denitrification process (Puig et al., 2011; Sabba et al., 2017; Cecconet et al., 2019). In previous study, denitrification with H_2 and CO_2 had a complete denitrification without intermediate nitrogen compounds accumulation under low nitrate (<100 mg/L) influent (Vasiliadou et al., 2006). Furthermore, other study (Lee and Rittmann, 2003) and our group studies (Xia et al., 2009; Zhang et al., 2009) found that denitrification with high pH (>9.2) would start to show the incomplete process with nitrite accumulation, but complete denitrification would achieved at low pH (ca. 7–8.5). Consequently, MBfR operated with low nitrate influent and low pH should have a complete denitrification process without intermediate nitrogen compounds accumulation.

3.2. Effect of nitrate on the ClO_4^- reduction process

Fig. 3 summarizes the effluent concentrations of ClO_4^- and Cl^-, the removal efficiencies of ClO_4^- and NO_3^--N, and the fluxes and normalized fluxes of ClO_4^- and NO_3^--N. As the influent NO_3^--N concentration increased from 1 to 5 mg/L, the effluent ClO_4^- concentration declined from 57 to 16 μg/L, and the ClO_4^- removal increased from 97% to 99%. Increasing the influent NO_3^--N concentration to 10 mg/L resulted in a slight increase of the effluent ClO_4^- concentration (34 μg/L). However, the ClO_4^- reduction process was enhanced due to the NO_3^--N addition, and higher removal and Cl^- conversion values were observed compared to values in stage 1. When 20 mg/L (stage 4) and 50 mg/L (stage 5) of NO_3^--N were introduced to the influent, the ClO_4^- removal sharply decreased to 81% and 63%, respectively, and the Cl^- conversion declined below 22%. These results clearly indicate that increasing the NO_3^--N loading moderately (<10 mg N/L or a ratio of NO_3^--N to ClO_4^- <5) promotes ClO_4^- reduction. In contrast, NO_3^- significantly inhibited ClO_4^- reduction at higher NO_3^--N loadings (>20 mg N/L or a ratio of NO_3^--N to ClO_4^- >10). Thus, the promotion or inhibition of denitrification on the ClO_4^- reduction process was controlled by the gradient of NO_3^--N loading. Similar results were obtained during the simultaneous removal of NO_3^- and ClO_4^- (Van Ginkel et al., 2008; Zhao et al., 2011; Tang et al., 2012a, 2012b; Zhu et al., 2016). Interestingly, the effect of NO_3^- on the bromate (BrO_3^-) reduction reported by previous study revealed a similar tendency (Downing and Nerenberg, 2007). Specifically, these authors found that low concentrations of NO_3^- provided the energy required for bromate-reducing bacteria to grow, while concentrations of NO_3^--N higher than 5 mg/L significantly inhibited BrO_3^- reduction.

From stage 1 to stage 5, the ClO_4^- flux declined from 0.0203 to 0.0132 $g/m^2 \cdot d$, whereas the normalized ClO_4^- flux increased from 0.3555 to 1.2512 m/d and then decreased to 0.0180 m/d. The denitrification flux gradually increased from 0.0107 to 0.4892 $g/m^2 \cdot d$, although the normalized NO_3^--N flux declined from 1.0716 to 0.1013 m/d. Unlike

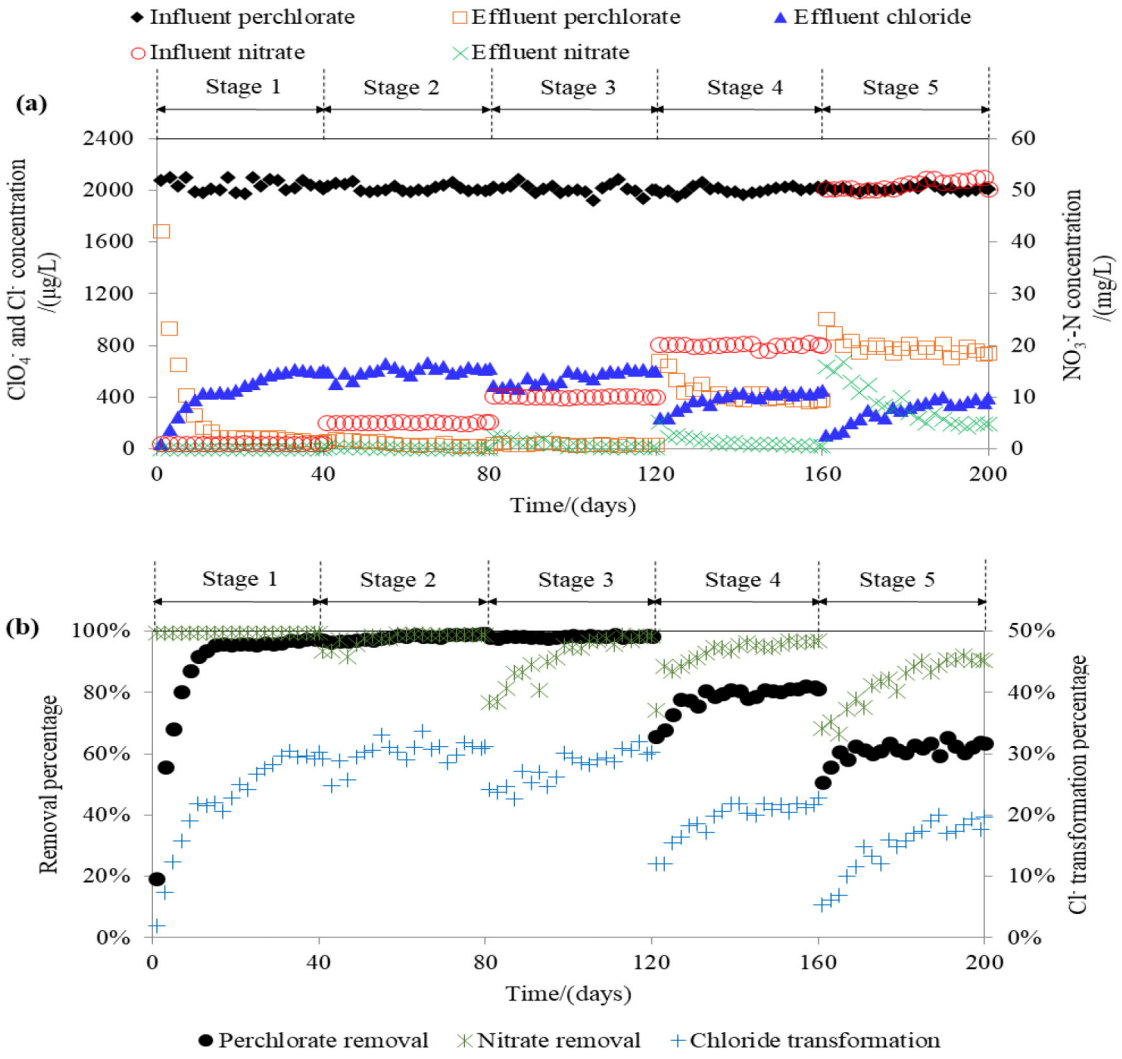

Fig. 2. Effluent concentrations of ClO_4^-, Cl^- and NO_3^--N (a), and ClO_4^- and NO_3^--N removal and Cl^- transformation percentages (b) during the five stages.

the ClO_4^- and NO_3^--N fluxes that experienced minor changes, the normalized ClO_4^- and NO_3^--N fluxes changed dramatically (Fig. 3). These results imply that ClO_4^- reduction was strongly affected by denitrification. ClO_4^- reduction rates were also reported to decrease as denitrification activity increased in some reactors (Zhao et al., 2011; Nerenberg and Rittmann, 2004). NO_3^-, as a primary electron acceptor, may outcompete ClO_4^- for limited H_2 availability in mixed-culture reactors, and competition for H_2 by denitrification may inhibit ClO_4^- reduction.

3.3. Analysis of the competition for H_2 availability

The electron-equivalent fluxes and H_2 fluxes of ClO_4^- and NO_3^--N at steady states during long-term experiments are summarized in Table 3. By comparing the actual H_2 consumption fluxes with the maximum H_2 diffusion flux (0.246 g of $H_2/m^2 \cdot d$), we observe that stages 1, 2, 3, and 4 had sufficient H_2 delivery and were therefore not limited by the electron donor. In contrast, stage 5 was H_2-limited because the actual H_2 flux (0.2211 g of $H_2/m^2 \cdot d$) was very close to the maximum H_2 flux. The high total H_2 flux and incomplete NO_3^- and ClO_4^- reduction processes clearly reveal that the biofilm was limited by H_2 delivery in stage 5.

Denitrification was the largest consumer of electrons (69.7–99.4%), and ClO_4^- reduction accounted for a small percentage of the electron fluxes (0.6–30.3%). These findings indicate that the total demand for H_2 was largely controlled by denitrification, which explains why the higher NO_3^--N loading only slightly changed the ClO_4^- fluxes and electron-equivalent fluxes. The electron-equivalent flux of ClO_4^- was negatively affected by low H_2 availability (especially in stage 5), along with a 0.6% percentage of ClO_4^- in total electron-equivalent fluxes. These results demonstrate that denitrification mainly used electrons from H_2 oxidation, regardless of the H_2 availability in the biofilm.

The biofilm reaction order (k') was calculated to investigate the sensitivity of the NO_3^- and ClO_4^- reduction process towards the H_2 competition and quantitatively describes the effects of NO_3^- on the ClO_4^- reduction. As shown in Fig. 4, the reaction orders of NO_3^- and ClO_4^- were 0.6083 and −0.1098, respectively, while the NO_3^--N concentration in the influent increased from 1 to 50 mg/L. These findings clearly suggest that denitrification competed more strongly for H_2 than ClO_4^- reduction. In other words, denitrification is more sensitive to changes in H_2 availability produced by high influent NO_3^--N loadings as compared to the ClO_4^- reduction. These results are consistent with the observed inhibition on ClO_4^- reduction when high NO_3^--N loadings were used (Figs. 2 and 3).

3.4. Analysis of the biofilm microbial community

Fig. 5(a) shows the taxonomic breakdown (at the class level) of all the biofilm sample communities at stages 1–5. *Betaproteobacteria* were the dominant bacteria, accounting for 69.9, 76.5, 87.1, 79.9, and 62.3%, respectively. When NO_3^- was added to the influent in stages 2–5, the abundance of *Betaproteobacteria* reached a maximum relative

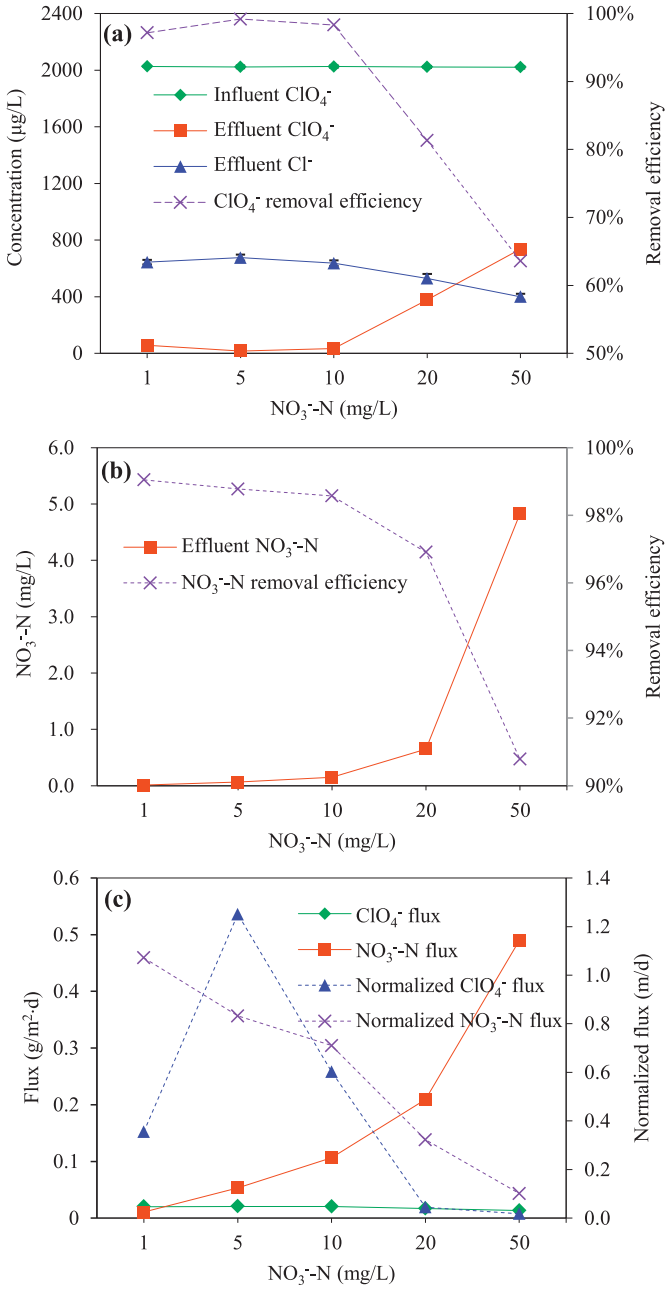

Fig. 3. Effect of the influent NO_3^--N concentration on ClO_4^- bioreduction: (a) influent ClO_4^- concentration, ClO_4^- and Cl^- concentrations in the effluent and ClO_4^- removal efficiency; (b) effluent NO_3^--N concentration and removal efficiency; (c) ClO_4^- and NO_3^--N fluxes, ClO_4^- and NO_3^--N fluxes normalized to the effluent ClO_4^- and NO_3^--N concentrations.

abundance of 87.1% and decreased thereafter. These values corresponded to variations in the ClO_4^- flux (Fig. 3). *Betaproteobacteria* have been widely reported to act as perchlorate reducers and denitrifiers and prevailed the biofilms during the simultaneous NO_3^- and ClO_4^- reduction processes (Zhao et al., 2011; Logan, 2001; Zhu et al., 2016). The abundance of *Alphaproteobacteria* increased from 3.8 to 20.8%, while the abundance of *Gammaproteobacteria* decreased from 11.1 to 5.1% with decreasing electron donors. The bacteria with the most powerful chlorate reducing activity was *Gammaproteobacteria* (Roldan et al., 1994), which led to incomplete ClO_4^- reduction in stages 4 and 5. The total abundance of *Proteobacteria* showed a similar trend to that of *Betaproteobacteria*. The community structure of the biofilm changed significantly as the influent NO_3^--N concentration increased.

Fig. 5(b) shows the relative proportions of the most abundant bacterial genera during the different stages. The genera *Methyloversatilis* (*Betaproteobacteria*), *Zoogloea* (*Betaproteobacteria*), *Citrobacter* (*Gammaproteobacteria*), *Limnohabitans* (*Betaproteobacteria*), *Acinetobacter* (*Gammaproteobacteria*), *Pseudomonas* (*Gammaproteobacteria*), *Hydrogenophaga* (*Betaproteobacteria*), *Dechloromonas* (*Betaproteobacteria*), and *Azospira* (*Betaproteobacteria*) were present in all stages. The genera *Methyloversatilis*, *Zoogloea*, and *Hydrogenophaga* were strongly enriched in the five stages, accounting for 31.9–56.5%, 10.6–25.8%, and 0.3–1.9%, respectively. The amounts of *Methyloversatilis*, *Zoogloea*, and *Hydrogenophaga* reached a maximum with the NO_3^--N concentration and decreased thereafter. *Methyloversatilis*, *Zoogloea*, and *Hydrogenophaga* have been widely reported as relevant denitrification bacteria (Zhang et al., 2009; Li et al., 2010; Sun et al., 2016; Li et al., 2018), while other researchers have found that *Methyloversatilis* and *Zoogloea* became dominant in autotrophic NO_3^-/ClO_4^- reducing reactors (Gao et al., 2015, 2016). Although the ability of *Methyloversatilis* and *Zoogloea* to reduce ClO_4^- was not clear, the reduction activity of these bacteria cannot be ruled out. Provided that *Methyloversatilis* and *Zoogloea* can utilize ClO_4^- as an electron acceptor, then the elevated relative abundance of *Methyloversatilis* and *Zoogloea* could account for the improved ClO_4^- removal in the H_2/CO_2-MBfR. In this study, changes in the amounts of *Methyloversatilis* and *Zoogloea* were consistent with changes in the ClO_4^- flux and removal efficiency. Thus, we suggest that *Methyloversatilis* and *Zoogloea* play an important role in ClO_4^- reduction. The genera *Citrobacter* (1.9–5.8%), *Limnohabitans* (3.4–4.3%), *Acinetobacter* (0.9–2.8%), *Pseudomonas*

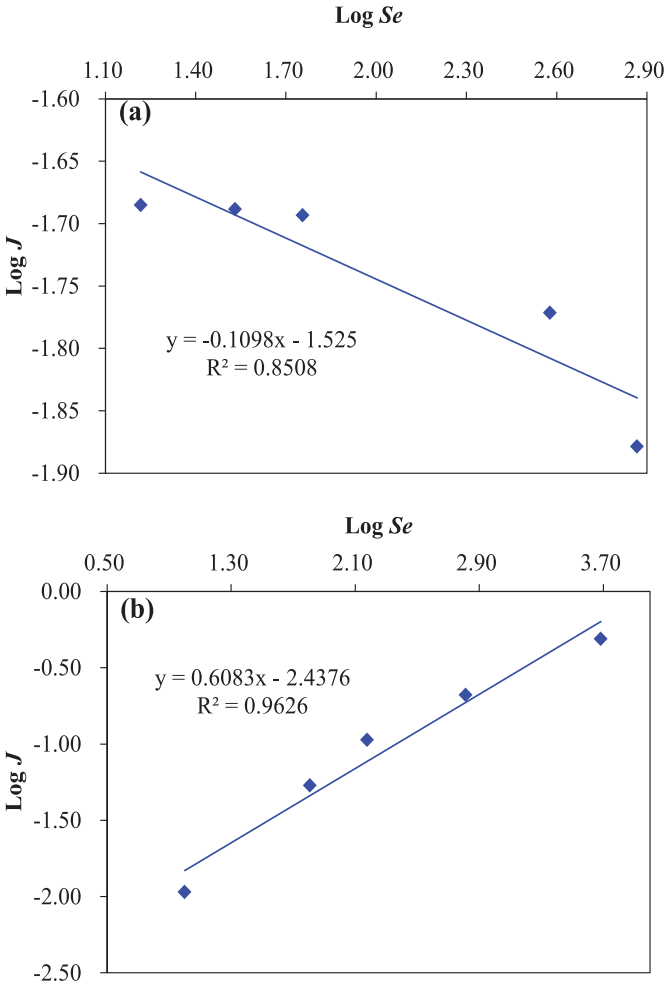

Fig. 4. Logarithm of: (a) ClO_4^- flux and (b) NO_3^--N flux plotted against the logarithm of the effluent ClO_4^- and NO_3^--N concentration.

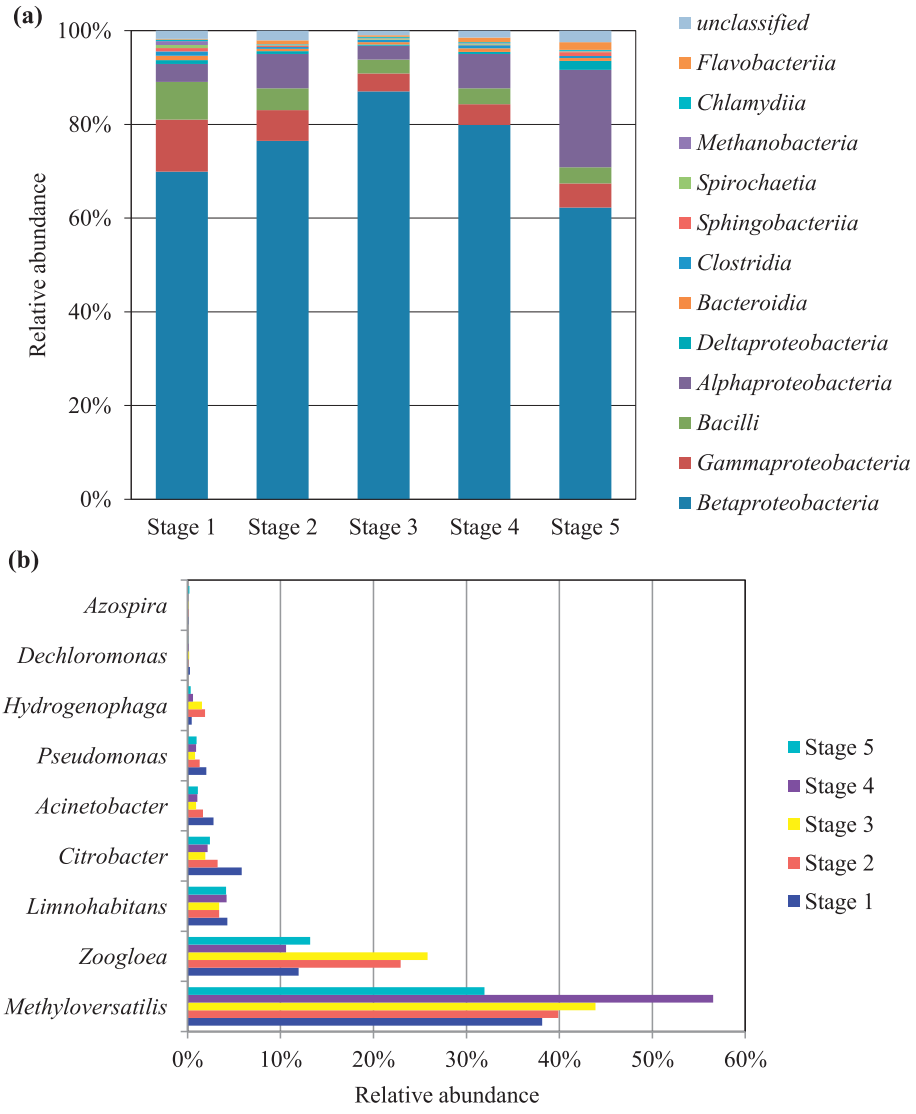

Fig. 5. Relative abundances of high-throughput sequences from biofilms at the class (a) and genus (b) levels for all five steady states.

(0.8–2.0%), *Dechloromonas* (0.1–0.3%), and *Azospira* (0.1–0.2%) use both NO_3^- and ClO_4^- as electron acceptors (Okeke et al., 2002; Coates and Achenbach, 2004; Guan et al., 2015). These bacteria were detected in all stages. However, their total proportions decreased sharply from 11.1 to 3.9%, and then slightly increased to 4.8% as the actual H_2 flux increased from 0.0191 to 0.2211 g $H_2/m^2 \cdot d$. This trend is opposite to that found for *Methyloversatilis*, *Zoogloea*, and *Hydrogenophaga*. Moreover, as the electron donors decreased, the H_2/CO_2-MBfR appeared to become more mixotrophic in stages 4 and 5, when heterotrophs became more selective as H_2 was more limited (especially in stage 5). Therefore, the addition of NO_3^- promoted the growth of perchlorate reducers, but insufficient or limiting levels of H_2 inhibited the development of bacteria involved in ClO_4^- reduction.

The variations of function genes at different stages were analyzed by high-throughput sequencing and KEGG annotation (Fig. 6). The analysis of functional genes in biofilms capable of degrading xenobiotics (pollutants) showed that the relative abundance of genes involved in the nitrogen cycle was 1.02–1.14% while that of the genes involved in the chlorine cycle was 0.77–0.91% (Fig. 7). The relative abundance of genes involved in the nitrogen cycle was close to that of genes involved in degrading chlorinated substances. It was speculated that the bacteria involved in the nitrogen and chlorine cycles jointly achieved the reductive degradation of ClO_4^-. Although the analysis of functional genes by KEGG annotation has some limitations, these results demonstrated that the degradation of ClO_4^- under complex conditions was carried out by a combination of various bacteria. Moreover, the biofilm community structure changed as a result of the addition of NO_3^-, ultimately becoming a suitable system for ClO_4^- degradation.

Fig. 8 shows the weighted PCoA based on the increased influent NO_3^--N concentration. Biofilm samples for stages 1–4 were grouped together and showed much higher PCoA1 values compared to stage 5. Clustering tree plot based on OTUs and values of Chao1, ACE, Shannon, and Simpson indexes also support this trend (Fig. S2 and Table S1). Thus, the higher influent loading of NO_3^--N (50 mg N/L) had a great impact on shaping the microbial communities of the biofilms, which may have inhibited ClO_4^- reduction. The community shifts shown by PCoA are related to the limitation of H_2 (i.e., insufficient electron donor) in the biofilm (Table 3). Moreover, the clear distinction of the PCoA2 vector between samples in stage 1 and stages 2–5 suggests that the microbial structure was also related to the addition of NO_3^--N to the flow. The feed composition and H_2 supply have been previously reported to promote shifts in the microbial community populations (Zhou et al.,

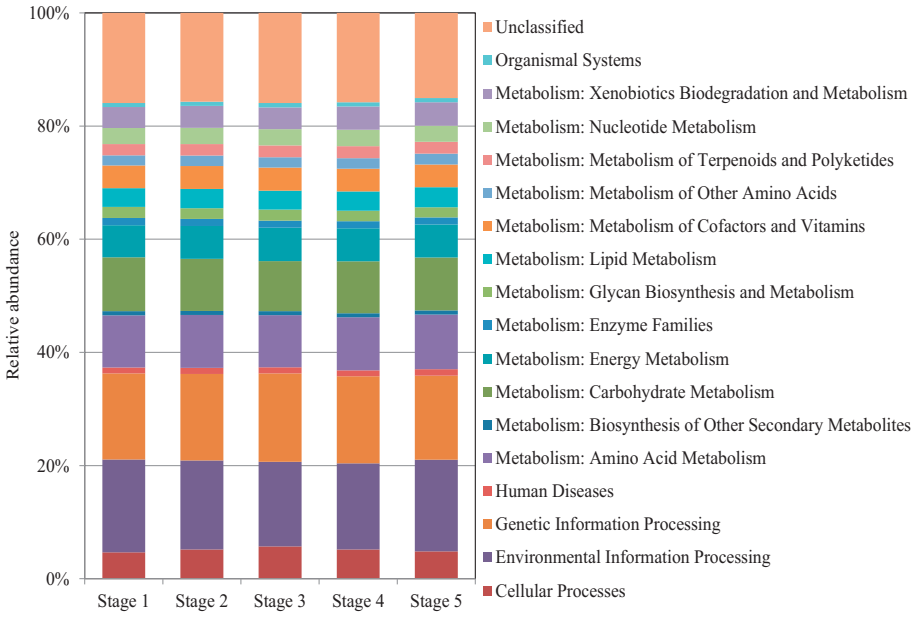

Fig. 6. Relative abundance of functional genes based on KEGG annotation.

2014; Ontiveros-Valencia et al., 2017). This study suggests that insufficient H_2 caused by higher NO_3^--N loading affected the community structure more significantly than the presence of NO_3^--N.

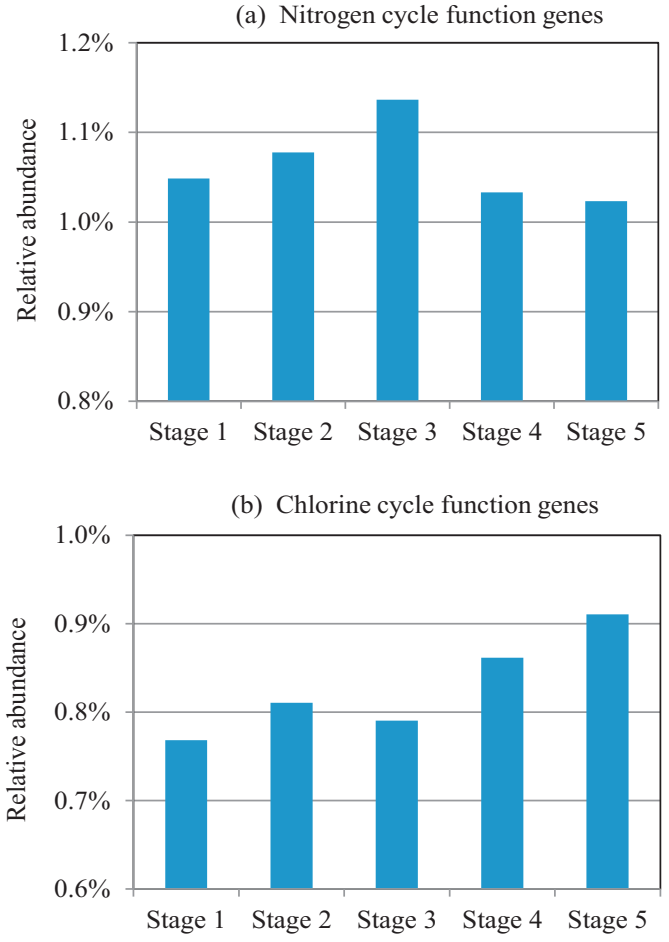

Fig. 7. Nitrogen cycle (a) and chlorine cycle (b) function genes by relative abundance in different.

3.5. Analysis of the mechanisms of NO_3^- influencing on ClO_4^- reduction

The results of this study showed that NO_3^- can promote ClO_4^- reduction at lower NO_3^--N loading levels, as well as inhibit ClO_4^- reduction at higher NO_3^--N loading levels (>20 mg N/L or a ratio of NO_3^--N to ClO_4^- >10). Several ClO_4^- reductions taking place in the presence of NO_3^- were previously attributed to NO_3^- supporting high growth rates of ClO_4^- reducers (Xu et al., 2004). Thus, enhanced ClO_4^- reduction rates can also be expected from cells grown in the presence of NO_3^-. This observation may be explained by two mechanisms: (1) a single ClO_4^- reducer can simultaneously catalyze the reduction of both ClO_4^- and NO_3^-; and (2) a single organism containing both ClO_4^- and NO_3^- reductases at different locations. The former is a co-metabolic mechanism for denitrification and ClO_4^- reduction, while the latter is an independent reduction mechanism for ClO_4^- reduction. As shown in Figs. 3, 5 and 7, the changes in the amount of *Methyloversatilis* and *Zoogloea*

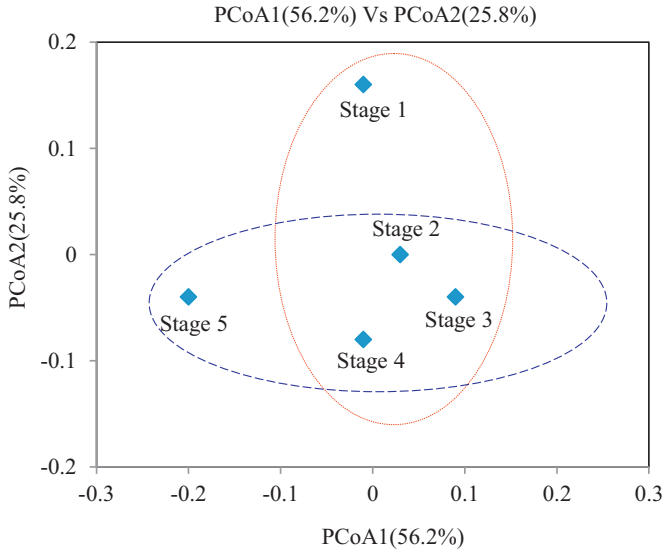

Fig. 8. PCoA based on weighted UniFrac analysis showing the microbial community grouping.

were consistent with changes in ClO_4^- fluxes and removal efficiencies, as well as with changes in the relative abundances of nitrogen cycle function genes. Thus, we speculate that *Methyloversatilis* and *Zoogloea* possess independent mechanisms capable of ClO_4^- reduction. The genera *Citrobacter*, *Acinetobacter*, *Pseudomonas*, *Dechloromonas*, and *Azospira* can co-metabolize both components. Moreover, an independent mechanism for ClO_4^- reduction dominated the total ClO_4^- removal in the reactor.

Two mechanisms may explain the strong inhibitory effect of NO_3^- on ClO_4^- reduction at higher NO_3^--N loadings. First, denitrification competed more strongly for H_2 as an electron donor than ClO_4^- reduction. As shown in Table 3, H_2 consumption in stage 5 was close to the theoretical maximum delivery capacity of the membrane, suggesting limited H_2 availability. Incomplete ClO_4^- removal (63%) and NO_3^--N removal (90%) provided further evidence of limited H_2 availability. Second, NO_3^- may cause a longer lag in ClO_4^- reduction (Tan et al., 2004), with ClO_4^- reduction starting only after the complete removal of NO_3^- because of the preferential NO_3^- utilization by microorganisms. Consequently, NO_3^- can suppress the ClO_4^- reductase activity and thus inhibit ClO_4^- removal. This inhibitory effect should increase with increasing NO_3^--N concentration in the reactor.

4. Conclusions

ClO_4^- was reduced significantly at influent NO_3^--N concentrations lower than 10 mg/L. NO_3^- promoted ClO_4^- reduction at ratios of NO_3^--N to ClO_4^- lower than 5, but inhibited ClO_4^- reduction at ratios higher than 10. Denitrification used most of the electrons from H_2 oxidation, regardless of the biofilm H_2 availability. Higher NO_3^--N loading generated insufficient H_2 in the biofilm, which shaped the biofilm community structure more strongly than the presence of NO_3^--N. High-throughput sequencing showed that *Betaproteobacteria* were dominant in all stages, and *Methyloversatilis*, *Zoogloea*, *Citrobacter*, *Acinetobacter*, *Pseudomonas*, *Dechloromonas*, and *Azospira* were genera involved in simultaneous ClO_4^- reduction and denitrification. *Methyloversatilis* and *Zoogloea* play important roles in ClO_4^- reduction.

Acknowledgements

This work was supported by the National Natural Science Foundation of China (51878197, 51768012, 51708362, and 51678422), the Guangxi Natural Science Foundation (2016GXNSFAA380204 and 2016GXNSFBA380207), the Guangxi Science and Technology Planning Project (GuiKe-AD18126018), the National Key Research and Development Program of China (2017YFC0403403), and the Special Funding for Guangxi 'Bagui Scholars' Construction Project. We would like to thank LetPub (www.letpub.com) for providing linguistic assistance during the preparation of this manuscript.

Appendix A. Supplementary data

Supplementary data to this article can be found online at https://doi.org/10.1016/j.scitotenv.2019.07.370.

References

Butler, C.S., Clauwaert, P., Green, S.J., Verstraete, W., Nerenberg, R., 2010. Bioelectrochemical perchlorate reduction in a microbial fuel cell. Environ. Sci. Technol. 44, 4685–4691.

Cao, F., Jaunat, J., Sturchio, N., Cancès, B., Morvan, X., Devos, A., Barbin, V., Ollivier, P., 2019. Worldwide occurrence and origin of perchlorate ion in waters: a review. Sci. Total Environ. 661, 737–749.

Cartier, T., Baert, A., Cabillic, P.J., Casellas, C., Creppy, E., Montiel, A., Pignatelli, B., Rosin, C., Sauvant-Rochat, M.P., Seux, R., Joyeux, M., 2012. Risk assessment of chemicals in drinking water: perchlorate and bromate. Environ. Risque. Sante 11 (4), 316–321.

Cecconet, D., Callegari, A., Capodaglio, A.G., 2018. Bioelectrochemical systems for removal of selected metals and perchlorate from groundwater: a review. Energies 11 (10), 2643.

Cecconet, D., Bolognesi, S., Callegari, A., Capodaglio, A.G., 2019. Controlled sequential biocathodic denitrification for contaminated groundwater bioremediation. Sci. Total Environ. 651, 3107–3116.

Choi, H., Silverstein, J., 2008. Inhibition of perchlorate reduction by nitrate in a fixed biofilm reactor. J. Hazard. Mater. 159 (30), 440–445.

Chung, J., Rittmann, B.E., 2007. Bio-reductive dechlorination of 1,1,1-trichloroethane and chloroform using a hydrogen based membrane biofilm reactor. Biotechnol. Bioeng. 97 (1), 52–60.

Coates, J.D., Achenbach, L.A., 2004. Microbial perchlorate reduction: rocket-fuelled metabolism. Nat. Rev. Microbiol. 2 (7), 569–580.

Downing, L.S., Nerenberg, R., 2007. Kinetics of microbial bromate reduction in a hydrogen-oxidizing, denitrifying biofilm reactor. Biotechnol. Bioeng. 98 (3), 543–550.

Fabro, A.Y.R., Avila, J.G.P., Alberich, M.V.E., Sansores, S.A.C., Camargo-Valero, M.A., 2015. Spatial distribution of nitrate health risk associated with groundwater use as drinking water in Merida, Mexico. Appl. Geogr. 65, 49–57.

Fan, A.M., Steinberg, V.E., 1996. Health implications of nitrate and nitrite in drinking water: an update on methemoglobinemia occurrence and reproductive and developmental toxicity. Regul. Toxicol. Pharma. 23, 35–43.

Gao, M., Wang, S., Jin, C., She, Z., Zhao, C., Zhao, Y., Zhang, J., Ren, Y., 2015. Autotrophic perchlorate reduction kinetics of a microbial consortium using elemental sulfur as an electron donor. Environ. Sci. Pollut. Res. 22 (13), 9694–9703.

Gao, M., Wang, S., Ren, Y., Jin, C., She, Z., Zhao, Y., Yang, S., Guo, L., Zhang, J., Li, Z., 2016. Simultaneous removal of perchlorate and nitrate in a combined reactor of sulfur autotrophy and electrochemical hydrogen autotrophy. Chem. Eng. J. 284, 1008–1016.

Guan, X., Xie, Y., Wang, J., Wang, J., Liu, F., 2015. Electron donors and co-contaminants affect microbial community composition and activity in perchlorate degradation. Environ. Sci. Pollut. Res. 22 (8), 6057–6067.

Herman, D.C., Frankenberger, W.T., 1999. Bacterial reduction of perchlorate and nitrate in water. J. Environ. Qual. 28 (3), 1018–1024.

Hutchison, J.M., Guest, J.S., Zilles, J.L., 2017. Evaluating the development of biocatalytic technology for the targeted removal of perchlorate from drinking water. Environ. Sci. Technol. 51 (12), 7178–7186.

Kimbrough, D.E., Parekh, P., 2007. Occurrence and co-occurrence of perchlorate and nitrate in California drinking water sources. J. Am. Water Works Ass. 99 (9), 126–132.

Lai, C.Y., Yang, X., Tang, Y., Rittmann, B.E., Zhao, H., 2014. Nitrate shaped the selenate-reducing microbial community in a hydrogen-based biofilm reactor. Environ. Sci. Technol. 48 (6), 3395–3402.

Lee, K.C., Rittmann, B.E., 2003. Effects of pH and precipitation on autohydrogenotrophic denitrification using the hollow-fiber membrane-biofilm reactor. Water Res. 37, 1551–1556.

Li, X., Upadhyaya, G., Yuen, W., Brown, J., Morgenroth, E., Raskin, L., 2010. Changes in the structure and function of microbial communities in drinking water treatment bioreactors upon addition of phosphorus. Appl. Environ. Microb. 76 (22), 7473–7481.

Li, H., Zhou, L., Lin, H., Xu, X., Jia, R., Xia, S., 2018. Dynamic response of biofilm microbial ecology to para-chloronitrobenzene biodegradation in a hydrogen-based, denitrifying and sulfate-reducing membrane biofilm reactor. Sci. Total Environ. 643, 842–849.

Logan, B.E., 2001. Assessing the outlook for perchlorate remediation. Environ. Sci. Technol. 35 (23), 482A–487A.

Logan, B.E., Lapoint, D., 2002. Treatment of perchlorate and nitrate-contaminated groundwater in an autotrophic, gas phase, packed-bed bioreactor. Water Res. 36 (14), 3647–3653.

London, M.R., De Long, S.K., Strahota, M.D., Katz, L.E., Speitel, G.E., 2011. Autohydrogenotrophic perchlorate reduction kinetics of a microbial consortium in the presence and absence of nitrate. Water Res. 45 (19), 6593–6601.

Nerenberg, R., Martin, K.J., 2012. The membrane biofilm reactor (MBfR) for water and wastewater treatment: principles, applications, and recent developments. Bioresour. Technol. 122 (S1), 83–94.

Nerenberg, R., Rittmann, B.E., 2004. Hydrogen-based, hollowfiber membrane biofilm reactor for reduction of perchlorate and other oxidized contaminants. Water Sci. Technol. 49, 223–230.

Okeke, B.C., Giblin, T., Frankenberger, W.T., 2002. Reduction of perchlorate an nitrate by salt tolerant bacteria. Environ. Pollut. 118 (3), 357–363.

Ontiveros-Valencia, A., Zhou, C., Ilhan, Z.E., Cyr, L.C.D.S., Krajmalnik-Brown, R., Rittmann, B.E., 2017. Total electron acceptor loading and composition affect hexavalent uranium reduction and microbial community structure in a membrane biofilm reactor. Water Res. 125, 341–349.

Puig, S., Serra, M., Vilar-Sanz, A., Cabre, M., Baneras, L., Colprim, J., 2011. Autotrophic nitrite removal in the cathode of microbial fuel cells. Bioresour. Technol. 102, 4462–4467.

Rittmann, B.E., McCarty, P.L., 2001. Environmental Biotechnology: Principles and Applications. McGraw-Hill Book Co, New York.

Roldan, M.D., Reyes, F., Morenovivian, C., Castillo, F., 1994. Chlorate and nitrate reduction in the phototrophic bacteria Rhodobacter capsulatus and Rhodobacter sphaeroides. Curr. Microbiol. 29 (4), 241–245.

Sabba, F., Picioreanu, C., Perez, J., Nerenberg, R., 2015. Hydroxylamine diffusion can enhance N_2O emissions in nitrifying biofilms: a modeling study. Environ. Sci. Technol. 49, 1486–1494.

Sabba, F., Picioreanu, C., Boltz, J.P., Nerenberg, R., 2017. Predicting N_2O emissions from nitrifying and denitrifying biofilms: a modeling study. Water Sci. Technol. 75, 530–538.

Scheytt, T.J., Freywald, J., Ptacek, C.J., 2011. Study of selected soil, ground, and surface water samples on perchlorate in Germany: first results. Grundwasser 16 (1), 37–43.

Sevdaa, S., Sreekishnanb, T.R., Pousc, N., Puigc, S., Pantd, D., 2018. Bioelectroremediation of perchlorate and nitrate contaminated water: a review. Bioresour. Technol. 255, 331–339.

Shea, C., Clauwaert, P., Verstraete, W., Nerenberg, R., 2008. Adapting a denitrifying biocathode for perchlorate reduction. Water Sci. Technol. 58, 1941–1946.
Sun, Y., Shen, D., Zhou, X., Shi, N., Tian, Y., 2016. Microbial diversity and community structure of denitrifying biological filters operated with different carbon sources. Springer Plus 5, 1752.
Tan, K., Anderson, T.A., Jackson, W.A., 2004. Degradation kinetics of perchlorate in sediments and soils. Water Air Soil Pollu 151 (1–4), 245–259.
Tang, Y., Zhao, H., Marcus, A.K., Krajmalnik-Brown, R., Rittmann, B.E., 2012a. A steady-state biofilm model for simultaneous reduction of nitrate and perchlorate, part 2: parameter optimization and results and discussion. Environ. Sci. Technol. 46 (3), 1608–1615.
Tang, Y., Zhou, C., Van Ginkel, S.W., Ontiveros-Valencia, A., Shin, J., Rittmann, B.E., 2012b. Hydrogen permeability of the hollow fibers used in H_2-based membrane biofilm reactors. J. Membrane Sci. 407–408 (s407–408), 176–183.
U.S. EPA, 2011. Fact Sheet, Final Regulatory Determination for Perchlorate. https://www.epa.gov/sites/production/files/2015-08/documents/epa815f11003.pdf.
Van Ginkel, S.W., Ahn, C.H., Badruzzaman, M., Robert, D.J., Lehman, G., Adham, S.S., Rittmann, B.E., 2008. Kinetics of nitrate and perchlorate reduction in ion-exchange brine using the membrane biofilm reactor (MBfR). Water Res. 42 (15), 4197–4205.
Vasiliadou, I.A., Pavlou, S., Vayenas, D.V., 2006. A kinetic study of hydrogenotrophic denitrification. Process Biochem. 41, 1401–1408.
Wan, D., Liu, Y., Wang, Y., Wang, H., Xiao, S., 2017. Simultaneous bio-autotrophic reduction of perchlorate and nitrate in a sulfur packed bed reactor: kinetics and bacterial community structure. Water Res. 108, 280–292.
Xia, S., Zhang, Y., Zhong, F., 2009. A continuous stirred hydrogen-based polyvinyl chloride membrane biofilm reactor for the treatment of nitrate contaminated drinking water. Bioresour. Technol. 100, 6223–6228.
Xia, S., Li, H., Zhang, Z., Zhang, Y., Yang, X., Jia, R., Xie, K., Xu, X., 2011. Bioreduction of para-chloronitrobenzene in drinking water using a continuous stirred hydrogen-based hollow fiber membrane biofilm reactor. J. Hazard. Mater. 192 (2), 593–598.
Xia, S., Wang, C., Xu, X., Tang, Y., Wang, Z., Gu, Z., Zhou, Y., 2015. Bioreduction of nitrate in a hydrogen-based membrane biofilm reactor using CO_2 for pH control and as carbon source. Chem. Eng. J. 276, 59–64.
Xia, S., Xu, X., Zhou, C., Wang, C., Zhou, L., Rittmann, B.E., 2016. Direct delivery of CO_2 into a hydrogen-based membrane biofilm reactor and model development. Chem. Eng. J. 290, 154–160.
Xu, J., Trimble, J.J., Steinberg, L., Logan, B.E., 2004. Chlorate and nitrate reduction pathways are separately induced in the perchlorate-respiring bacterium Dechlorosoma sp. KJ and the chlorate-respiring bacterium Pseudomonas sp. PDA. Water Res. 38 (3), 673–680.
Ye, L., You, H., Yao, J., Su, H.L., 2012. Water treatment technologies for perchlorate: a review. Desalination 298, 1–12.
Zhang, Y., Zhong, F., Xia, S., Wang, X., Li, J., 2009. Autohydrogenotrophic denitrification of drinking water using a polyvinyl chloride hollow fiber membrane biofilm reactor. J. Hazard. Mater. 170 (1), 203–209.
Zhao, H., Van Ginkel, S.W., Tang, Y., Kang, D.W., Rittmann, B.E., Krajmalnik-Brown, R., 2011. Interactions between perchlorate and nitrate reductions in the biofilm of a hydrogen-based membrane biofilm reactor. Environ. Sci. Technol. 45 (23), 10155–10162.
Zhao, H., Ontiveros-Valencia, A., Tang, Y., Kim, B.O., Ilhan, Z.E., Krajmalnik-Brown, R., Rittmann, B., 2013. Using a two-stage hydrogen-based membrane biofilm reactor (MBfR) to achieve complete perchlorate reduction in the presence of nitrate and sulfate. Environ. Sci. Technol. 47 (3), 1565–1572.
Zhou, C., Ontiveros-Valencia, A., Cyr, L.C.D.S., Zevin, A.S., Carey, S.E., Krajmalnik-Brown, R., Rittmann, B.E., 2014. Uranium removal and microbial community in a H2-based membrane biofilm reactor. Water Res. 64 (22), 255–264.
Zhou, C., Ontiveros-Valencia, A., Wang, Z., Maldonado, J., Zhao, H., Krajmalnik-Brown, R., Rittmann, B.E., 2016. Palladium recovery in a H2-based membrane biofilm reactor: formation of Pd(0) nanoparticles through enzymatic and autocatalytic reductions. Environ. Sci. Technol. 50 (5), 2546–2555.
Zhu, Y., Wu, M., Gao, N., Chu, W., Wang, S., 2016. Impacts of nitrate and electron donor on perchlorate reduction and microbial community composition in a biologically activated carbon reactor. Chemosphere 165, 134–143.